



ACADÉMIE
DES SCIENCES
INSTITUT DE FRANCE

Comptes Rendus

Chimie

Simon Larsen, Jeanet Conradie, Nicolas Desbois, Claude Philippe Gros
and Abhik Ghosh


Hypsochlorins

Published online: 19 March 2024

Part of Special Issue: French/Nordic Special Issue on Materials and Coordination
Chemistry

Guest editors: Claude P. Gros (Université de Bourgogne, Dijon, France) and Abhik
Ghosh (The Arctic University, UiT, Tromsø, Norway)

<https://doi.org/10.5802/crchim.299>

 This article is licensed under the
CREATIVE COMMONS ATTRIBUTION 4.0 INTERNATIONAL LICENSE.
<http://creativecommons.org/licenses/by/4.0/>



*The Comptes Rendus. Chimie are a member of the
Mersenne Center for open scientific publishing*
www.centre-mersenne.org — e-ISSN : 1878-1543



Preliminary communication

French/Nordic Special Issue on Materials and Coordination Chemistry

Hypsochlorins

Simon Larsen^{Ⓜ, a}, Jeanet Conradie^{Ⓜ, a, b}, Nicolas Desbois^{Ⓜ, c}, Claude Philippe Gros^{Ⓜ, *, c}
and Abhik Ghosh^{Ⓜ, *, a}

^a Department of Chemistry, UiT – The Arctic University of Norway, Tromsø N-9037, Norway

^b Department of Chemistry, University of the Free State, Bloemfontein 9300, Republic of South Africa

^c Institut de Chimie Moléculaire de l'Université de Bourgogne (ICMUB), UMR CNRS 6302, Université de Bourgogne, 9 Avenue Alain Savary, BP 47870, 21078 Dijon Cedex, France

E-mails: claude.gros@u-bourgogne.fr (C. P. Gros), abhik.ghosh@uit.no (A. Ghosh)

Abstract. Both the Soret and Q bands of chlorin e6 complexes blueshift on going from Zn to Pd to Pt as the coordinated metal, establishing the latter two complexes as hypsochlorins. DFT/TDDFT calculations indicate that the blueshifts appear to be related to the presence of the electronegative metal ion, which lowers the orbital energies of the HOMO and HOMO-1, while leaving the LUMOs relatively unaffected.

Keywords. Chlorin, Hypsochlorin, Hypso, Hypso porphyrin, TDDFT.

Funding. Research Council of Norway (Grant no. 262229), CNRS (Grant no. UMR UBCNRS 6302), South African National Research Foundation (Grant nos. 129270 and 132504).

Manuscript received 29 September 2023, revised 10 January 2024, accepted 8 February 2024.

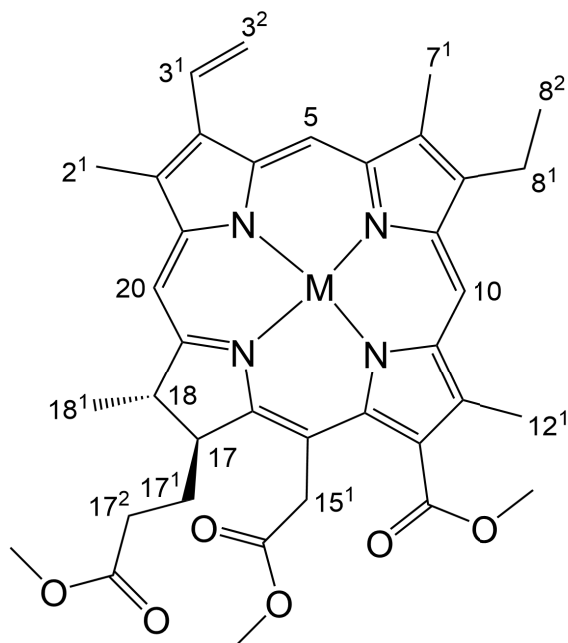
1. Introduction

Over a half-century ago, Martin Gouterman [1] devised his eponymous four-orbital model of porphyrin spectra, and thereby was able to classify them as belonging to three broad classes, normal, hyper and hypso [2,3]. Briefly, hyper spectra exhibit redshifted features and/or extra features relative to normal spectra, while hypso spectra are blueshifted relative to normal spectra. Although the variety of porphyrinoid compounds is vastly greater today, Gouterman's classification remains useful. Thus, the hyperporphyrin concept has emerged as a design principle for photosensitizers for photodynamic therapy and

related applications [4]. Many hypso porphyrins are phosphorescent and potentially useful as triplet photosensitizers, in such applications as oxygen sensing and photodynamic and related therapies [5–7]. The hypso effect had long been attributed to an increase in the HOMO–LUMO gap in certain late transition porphyrins as a result of antibonding interactions between occupied metal d_{π} orbitals and the porphyrin's e_g LUMOs. A recent DFT investigation, however, has indicated a different origin for the hypso effect, namely, a lowering of the a_{2u} HOMOs in metalloporphyrins with relatively electronegative metal ions such as Pd(II) and Pt(II) [8].

Many years ago, we showed that Gouterman's four-orbital model also applies to corroles [9,10]. Unsurprisingly, many metalcorroles exhibit hyper spectra [11–13] and quite a few also exhibit hypso

* Corresponding authors.



Scheme 1. A chlorin e6 trimethyl ester metal complex with partial atom numbering.

spectra [8]. Herein we show that the hypso effect also applies to chlorins [14,15], with both the Soret and Q band maxima of chlorins blueshifting, going from Zn to Pd to Pt as the coordinated metal (Scheme 1). The finding is surprising in that the HOMO of closed-shell chlorins is invariably an a_{1u} -type MO (in terms of D_{4h} irreps) [3,16–19] which has no amplitude on the central nitrogen atoms and is, therefore, likely to be unaffected by the electronegativity of the central metal. Gratifyingly, the spectral data proved consistent with electrochemical cyclic voltammetry measurements and DFT/TDDFT calculations, leading to a coherent picture of hypsochlorins, as described below.

2. Results and discussion

Table 1 lists the UV-vis absorption maxima and redox potentials (V versus SCE) of the Zn, Pd, and Pt complexes of chlorin e6 trimethyl ester, $M[\text{Chl-e}]$, where $M = \text{Zn, Pd, and Pt}$; the UV-vis spectra and cyclic voltammograms are depicted in Figures 1 and 2, respectively. From Zn to Pd and from Pd to Pt, the Q band blueshifts by 14 and 10 nm, respectively, and

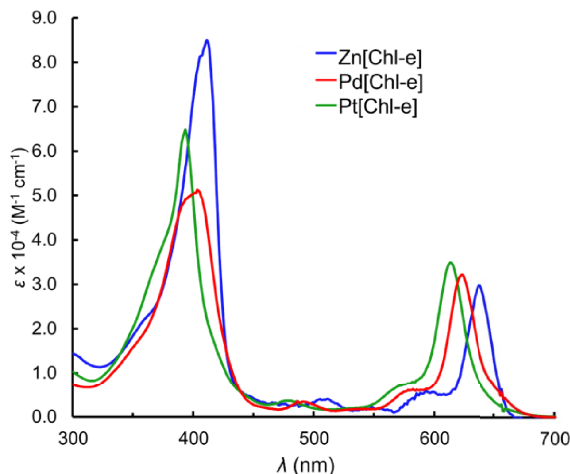


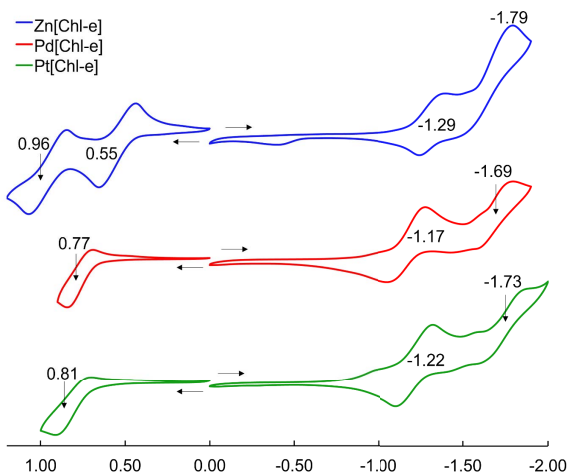
Figure 1. UV-visible spectra of $M[\text{Chl-e}]$, where $M = \text{Zn, Pd, and Pt}$, in CH_2Cl_2 at ambient temperature.

the Soret by 8 and 10 nm, respectively. The two minor features between the Soret and Q bands also blueshift in the same order. All complexes exhibit reversible 1st oxidations and 1st reductions. While there are small variations in the 1st reduction potentials there are greater variations in the 1st oxidation potentials and a clear trend of increasing oxidation potentials in the order of $\text{Zn} < \text{Pd} < \text{Pt}$, which in turn results in an increasing electrochemical HOMO–LUMO gap for the same series. The electrochemical data thus suggests that the hypso effect in chlorins stems primarily from a lowering of the HOMO energy in the presence of an electronegative coordinated metal.

To obtain a qualitative understanding of the above findings, DFT and TDDFT calculations were carried out using simple unsubstituted chlorin models of the complexes studied. The OLYP [20,21]-D3 [22]/ZORA-STO-TZ2P optimized geometries of $M[\text{Chl}]$ ($M = \text{Zn, Pd, Pt}$; $\text{Chl} = \text{unsubstituted chlorin}$; Figure 3) revealed essentially planar (as opposed to ruffled) geometries so differences in macrocycle conformation appear unlikely to be a significant contributor to the observed spectral differences [23]. Single-point CAMY-B3LYP [24] calculations were then carried out on the OLYP-D3 geometries. Figure 4 depicts selected CAMY-B3LYP frontier MOs along with the corresponding orbital energies, while Figure 5

Table 1. Redox potentials (V versus SCE) and UV-vis absorption maxima of the compounds studied

Compound	$E_{1/2ox2}$	$E_{1/2ox1}$	$E_{1/2red1}$	$E_{1/2red2}$	E_{red2}	ΔE	Soret band (nm)	Q band (nm)
Zn[Chl-e]	0.96	0.55	-1.29	-	-1.79	1.84	411	637
Pd[Chl-e]	-	0.77	-1.17	-1.69	-	1.94	403	623
Pt[Chl-e]	-	0.81	-1.22	-1.73	-	2.03	393	613

**Figure 2.** Cyclic voltammograms (V versus SCE) of M[Chl-e], where M = Zn, Pd, and Pt, in CH_2Cl_2 containing 0.1 M tetrabutylammonium perchlorate at ambient temperature; scan rate $100 \text{ mV}\cdot\text{s}^{-1}$.

presents the orbital energy levels in a graphical manner. Figure 6 depicts the simulated TD-CAMY-B3LYP-D3/Q4 STO-TZ2P-COSMO optical spectra in dichloromethane of the three M[Chl] derivatives. The key result is that, while the LUMO and LUMO+1 energies are essentially constant across all three M[Chl] derivatives, both the HOMO and HOMO-1 energies downshift going from Zn to Pd to Pt. Understandably, the downshifts for the a_{1u} -type HOMO are smaller than those for the a_{2u} -type HOMO-1, given that only the latter has substantial amplitudes on the central nitrogen atoms. In spite of the simplicity of our models, these computational results appear to nicely, if qualitatively, capture the essence of both the UV-vis and electrochemical measurements.

Finally, the calculated absorption maxima from CAMY-B3LYP TDDFT calculations on M[Chl] in dichloromethane (Figure 6) were found to be in

surprisingly good agreement with the experimental absorption maxima for M[Chl-e]. Thus, for instance, the calculations correctly captured the larger hypsochromic shifts for the Q band relative to the Soret band. In all three cases, the Q band consists of approximately 95% HOMO \rightarrow LUMO character, with the remainder made up of HOMO-1 \rightarrow LUMO+1 character (Table 2). The Soret band, by comparison, consists of a mixture of HOMO-1 \rightarrow LUMO and HOMO \rightarrow LUMO+1 character. Since both the HOMO and HOMO-1 downshift from Zn through Pd to Pt, it makes sense that both the Q and Soret absorption maxima blueshift in the same order.

In summary, a combined experimental and theoretical study indicates the plausible occurrence of a hypso effect in chlorins. Thus, both the Soret and Q bands blueshift going from Zn to Pd to Pt as the coordinated metal. As in the case of porphyrins, the blueshifts appear to be largely attributable to the presence of an electronegative coordinated atom, which lowers the orbital energies of the HOMO and HOMO-1, while leaving the LUMOs relatively unaffected.

3. Experimental section

3.1. Materials

All reagents were purchased from Sigma-Aldrich and used as received except chlorin e6 trimethyl ester (CAS 35038-32-5) which was purchased from PorphyChem. Silica gel 60 (0.04–0.063 mm particle size, 230–400 mesh, Merck) was employed for flash chromatography. Silica gel 60 preparative thin-layer chromatographic plates (20 cm \times 20 cm \times 0.5 mm, Merck) were used for final purification of all compounds.

3.2. General instrumental methods

UV-visible spectra were recorded on an HP 8454 spectrophotometer. ^1H NMR spectra were recorded

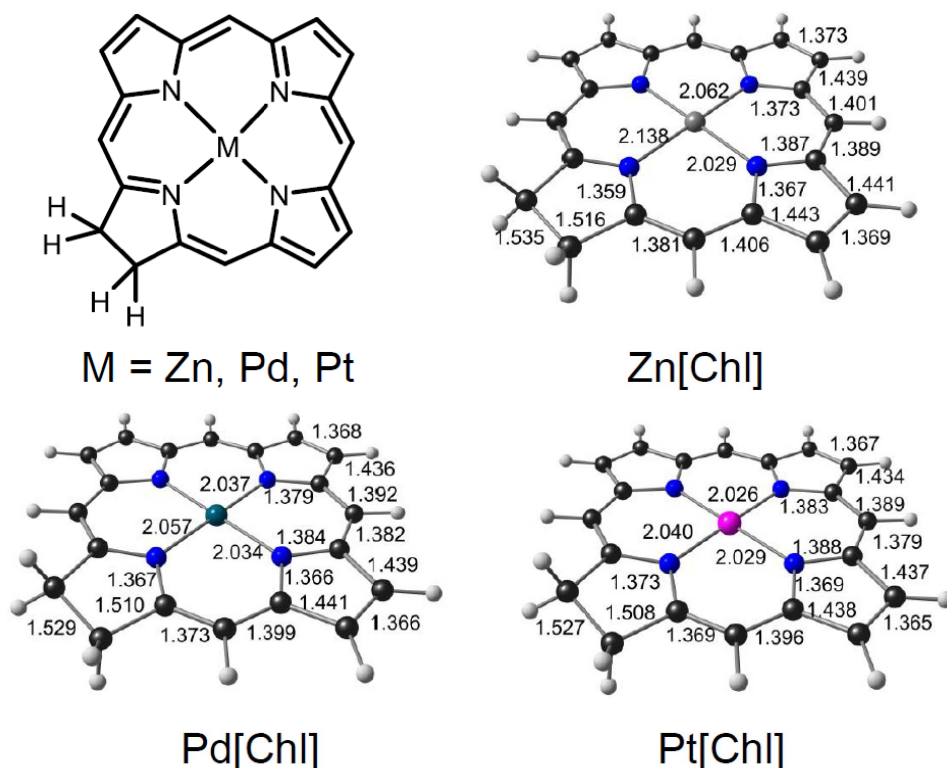


Figure 3. Selected skeletal bond distances for M[Chl], where M = Zn, Pd, and Pt and Chl = unsubstituted chlorin.

on a 400 MHz Bruker Avance III HD spectrometer equipped with a 5 mm BB/1H SmartProbe and referenced to either residual C_6H_6 at 7.16 ppm or residual $CHCl_3$ at 7.26 ppm. High-resolution electrospray-ionization mass spectra were recorded on an Orbitrap Exploris 120 spectrometer using methanolic solutions. Cyclic voltammetry was carried out at ambient temperature with a Gamry Reference 620 potentiostat equipped with a three-electrode system: a 3 mm disc glassy carbon working electrode, a platinum wire counter-electrode, and a saturated calomel reference electrode (SCE). Tetra(*n*-butyl)ammonium perchlorate (*CAUTION!*) was used as the supporting electrolyte. Anhydrous CH_2Cl_2 (Sigma-Aldrich) was used as solvent. The electrolyte solution was purged with argon for at least 2 min prior to all measurements, which were carried out under an argon blanket. The glassy carbon working electrode was polished using a polishing pad and 0.05 micrometer polishing alumina

from ALS Japan. All potentials were referenced to the SCE.

3.3. Synthesis

The Zn complex was made by adding a solution of $Zn(OAc)_2 \cdot 2H_2O$ (29.5 mg, 4 eq.) in 1 mL MeOH to a solution of chlorin e6 trimethyl ester (21.9 mg) in 5 mL chloroform. The resulting solution was refluxed for 1 h. The Pd complex was made by dissolving chlorin e6 trimethyl ester (17.3 mg) and $Pd(OAc)_2$ (19.7 mg, 3 eq.) in 5 mL pyridine and refluxing the resulting solution for 4 h. The Pt complex was made by dissolving chlorin e6 trimethyl ester (18.0 mg) and $Pt(OAc)_2$ (26.3 mg, 3 eq.) in 5 mL benzonitrile and refluxing the resulting solution for 10 h. Following reflux, each mixture was rotary-evaporated to dryness and the residue dissolved in DCM and placed on a silica column. Dichloromethane/ethyl acetate 20:1 eluted a blue fraction which was evaporated to

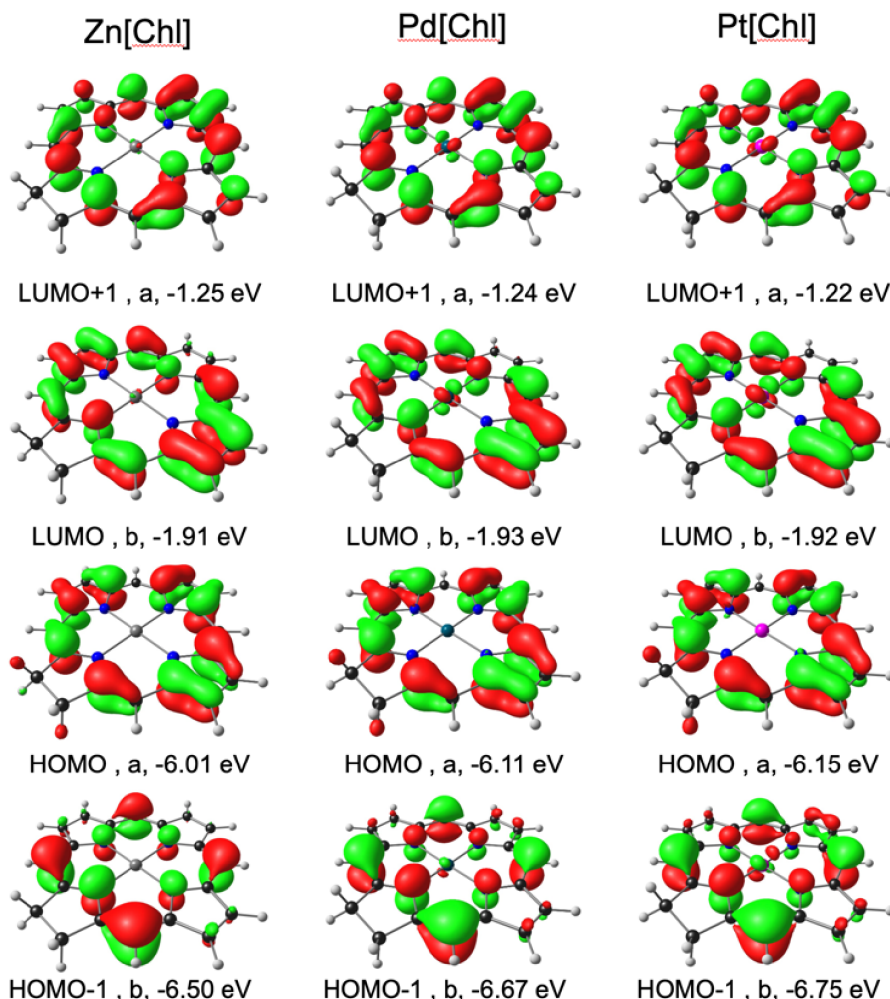


Figure 4. CAMY-B3LYP frontier MOs of M[Chl] (M = Zn, Pd, Pt), with C₂ irreps (a and b) and orbital energies.

dryness and further purified by preparative TLC using *n*-hexane/ethyl acetate 1:1 as solvent. Yields and analytical details are as follows:

3.3.1. Zn[Chl-*e*]

Yield 16.8 mg, 70%. UV-Vis (CH₂Cl₂) λ_{\max} (nm) [$\epsilon \times 10^{-4}$ (M⁻¹·cm⁻¹): 411 (8.50), 505 (0.40), 593 (0.58), 637 (2.98). ¹H NMR (400 MHz, C₆D₆, δ in ppm): 9.54 (s, 1H, **5**), 9.41 (s, 1H, **10**), 8.50 (s, 1H, **20**), 8.05 (dd, $J = 17.8, 11.5$ Hz, 1H, **3**¹), 6.18 (d, $J = 18.0$ Hz, 1H, **3**² *trans*), 5.91 (d, $J = 1.8$ Hz, 1H, **3**² *cis*), 5.45 (d, $J = 19.0$ Hz, 1H, **15**¹), 5.28 (d, $J = 19.0$ Hz, 1H, **15**¹), 4.28 (d, $J = 10.2$ Hz, 1H, **17**), 4.01 (t, $J = 7.1$ Hz, 1H, **18**), 3.95 (s, 3H, OCH₃), 3.59 (s, 3H, OCH₃), 3.47

(q, $J = 7.5$ Hz, 2H, **8**¹), 3.38 (s, 3H, OCH₃), 3.26 (s, 3H, **12**¹), 3.25 (s, 3H, **2**¹), 3.01 (s, 3H, **7**¹), 2.30 (dt, $J = 15.9, 7.9$ Hz, 1H, **17**¹), 2.07 (d, $J = 10.0$ Hz, 1H, **17**¹), 2.00–1.91 (m, 1H, **17**²), 1.67 (d, $J = 7.2$ Hz, 3H, **18**¹), 1.60 (t, $J = 7.6$ Hz, 3H, **8**²), ~1.55 (1H, **17**² concealed by overlapping peaks). MS (ESI, positive mode): m/z calcd for C₃₇H₄₀N₄O₅ZnH 701.2312; [M + H⁺] found 701.2307.

3.3.2. Pd[Chl-*e*]

Yield 1.9 mg, 9.4%. UV-Vis (CH₂Cl₂) λ_{\max} (nm) [$\epsilon \times 10^{-4}$ (M⁻¹·cm⁻¹): 403 (5.14), 486 (0.35), 582 (0.62), 623 (3.22). ¹H NMR (400 MHz, CDCl₃, δ in ppm): 9.57 (s, 1H, **5/10**), 9.56 (s, 1H, **5/10**), 8.62

Table 2. CAMY-B3LYP-D3/STO-TZ2P TDDFT results, including transition energies (E) and wavelengths (λ), oscillator strengths (f), MO compositions, and symmetries

Molecule	Peak	E (eV)	λ (nm)	f	MO composition			State symmetry
					From	To	Weight (%)	
Zn[Chl]	Q	2.12	584.6	0.45	HOMO	LUMO	92.6	B
					HOMO-1	LUMO+1	6.3	B
	Soret	3.04	408.4	1.80	HOMO	LUMO+1	62.3	A
					HOMO-1	LUMO	35.8	A
					HOMO-1	LUMO+1	91.4	B
		3.33	372.3	1.23	HOMO	LUMO	6.4	B
Pd[Chl]	Q	2.18	568.4	0.48	HOMO	LUMO	94.3	B
					HOMO-1	LUMO+1	4.5	B
	Soret	3.11	398.7	1.60	HOMO-1	LUMO	59.8	A
					HOMO	LUMO+1	38.2	A
					HOMO-1	LUMO+1	92.5	B
		3.47	356.9	1.10	HOMO	LUMO	4.5	B
Pt[Chl]	Q	2.23	556.1	0.50	HOMO	LUMO	94.8	B
					HOMO-1	LUMO+1	3.9	B
	Soret	3.18	390.1	1.58	HOMO	LUMO+1	56.5	A
					HOMO-1	LUMO	40.9	A
					HOMO-1	LUMO+1	92.6	B
		3.56	348.4	1.14	HOMO	LUMO	3.8	B

(s, 1H, **20**), 7.98 (dd, $J = 17.8, 11.5$ Hz, 1H, **3¹**), 6.16 (dd, $J = 17.8, 1.7$ Hz, 1H, **3² trans**), 6.03 (dd, $J = 11.5, 1.7$ Hz, 1H, **3² cis**), 5.14 (d, $J = 19.1$ Hz, 1H, **15¹**), 4.93 (d, $J = 19.0$ Hz, 1H, **15¹**), 4.48–4.35 (m, 2H, overlapping **17** and **18**), 4.19 (s, 3H, **OCH₃**), 3.86 (s, 3H, **OCH₃**), 3.75 (q, $J = 7.6$ Hz, 2H, **8¹**), 3.62 (s, 3H, **OCH₃**), 3.44 (s, 3H, **12¹**), 3.33 (s, 3H, **2¹**), 3.29 (s, 3H, **7¹**), 2.58–2.46 (m, 1H, **17¹**), 2.24–2.11 (m, 1H, **17¹**), 2.07–1.95 (m, 1H, **17²**), 1.75 (d, $J = 7.1$ Hz, 3H, **18¹**), 1.69 (t, $J = 7.6$ Hz, 3H, **8²**) ~1.69 (1H, **17²** concealed by overlapping peaks). MS (APCI, positive mode): m/z calcd for $C_{37}H_{40}N_4O_5PdH$ 743.2055; $[M + H^+]$ found 743.2065.

3.3.3. Pt[Chl-*e*]

Yield 5.8 mg, 24.7%. UV-Vis (CH_2Cl_2) λ_{max} (nm) [$\epsilon \times 10^{-4}$ ($M^{-1}\cdot cm^{-1}$): 393 (6.49), 478 (0.36), 613 (3.49). ¹H NMR (400 MHz, $CDCl_3$, δ in ppm): 9.56 (s, 1H, **5**), 9.52 (s, 1H, **10**), 8.70 (s, 1H, **20**), 7.98 (dd, $J = 17.8, 11.5$ Hz, 1H, **3¹**), 6.14 (dd, $J = 17.8, 1.7$ Hz,

1H, **3² trans**), 6.02 (dd, $J = 11.4, 1.6$ Hz, 1H, **3² cis**), 5.13 (d, $J = 19.1$ Hz, 1H, **15¹**), 4.93 (d, $J = 19.1$ Hz, 1H, **15¹**), 4.46–4.34 (m, 2H, overlapping **17** and **18**), 4.20 (s, 3H, **OCH₃**), 3.87 (s, 3H, **OCH₃**), 3.71 (q, $J = 7.6$ Hz, 2H, **8¹**), 3.63 (s, 3H, **OCH₃**), 3.50 (s, 3H, **12¹**), 3.31 (s, 3H, **2¹**), 3.24 (s, 3H, **7¹**), 2.54 (ddd, $J = 16.1, 9.0, 7.0$ Hz, 1H, **17¹**), 2.20 (ddd, $J = 16.2, 7.2, 4.8$ Hz, 1H, **17¹**), 2.09–1.97 (m, 1H, **17²**), 1.76 (d, $J = 7.1$ Hz, 3H, **18¹**), 1.68 (t, $J = 7.6$ Hz, 3H, **8²**), ~1.71 (1H, **17²** concealed by overlapping peaks). MS (APCI, positive mode): m/z calcd for $C_{37}H_{40}N_4O_5PtH$ 832.2668; $[M + H^+]$ found 832.2670.

3.4. Computational method

The three M[Chl] (M = Zn, Pd, Pt) complexes were optimized with scalar-relativistic DFT calculations, with the OLYP [20,21] functional augmented with Grimme's D3 [22] dispersion correction, all-electron ZORA STO-TZ2P basis sets, fine integration grids,

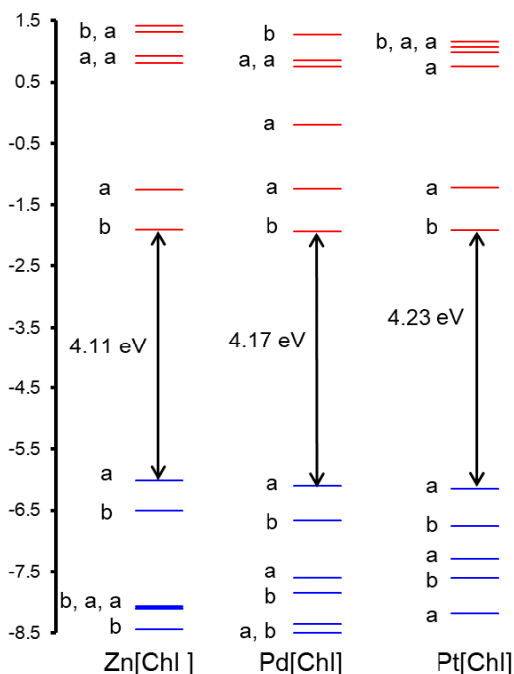


Figure 5. CAMY-B3LYP-D3/STO-TZ2P-COSMO frontier MO energy levels along with C_2 irreps (a and b).

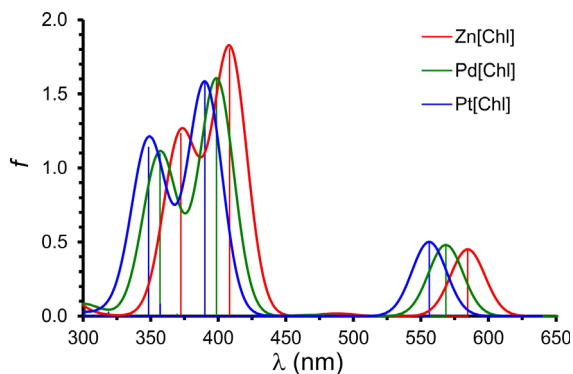


Figure 6. Simulated TD-CAMY-B3LYP-D3/STO-TZ2P-COSMO optical spectra in dichloromethane. The vertical lines represent calculated transitions which have then been broadened with Gaussians to generate the simulated spectra.

and tight criteria for both SCF cycles and geometry optimizations, as implemented in the ADF 2019 program system [25]. All the optimizations were carried out with a C_2 symmetry constraint and the

COSMO (Conductor like Screening Model) [26] solvation model with dichloromethane as solvent. TDDFT calculations were performed on the OLYP-D3 optimized geometries using the CAMY-B3LYP [24] range-separated functional (which has been extensively calibrated for calculations of porphyrin spectra [4,7,27]), with basis set and other parameters the same as in the ground-state calculations).

Declaration of interests

The authors do not work for, advise, own shares in, or receive funds from any organization that could benefit from this article, and have declared no affiliations other than their research organizations.

Funding

This research was supported by the Research Council of Norway (grant no. 262229 to AG), the CNRS (grant UMR UBCNRS 6302), and the South African National Research Foundation (grant nos. 129270 and 132504 to JC).

Acknowledgment

The authors also warmly thank Mrs. Sandrine Pacquelet for technical assistance.

Supplementary data

Supporting information for this article is available on the journal's website under <https://doi.org/10.5802/crchim.299> or from the author.

References

- [1] A. Ghosh, *Angew. Chem. Int. Ed.*, 2021, **60**, 9760-9770.
- [2] M. Gouterman, G. H. Wagnière, L. C. Snyder, *J. Mol. Spectrosc.*, 1963, **11**, 108-115.
- [3] M. Gouterman, in *The Porphyrins* (D. Dolphin, ed.), vol. III, Part A, Academic Press, New York, 1978, 1-165.
- [4] C. C. Wamser, A. Ghosh, *JACS Au*, 2022, **2**, 1543-1560.
- [5] Y. Lin, T. Zhou, R. Bai, Y. Xie, *J. Enzyme Inhib. Med.*, 2020, **35**, 1080-1099.
- [6] K. C. Tong, D. Hu, P. K. Wan, C. N. Lok, C. M. Che, *Adv. Inorg. Chem.*, 2020, **75**, 87-119.
- [7] A. B. Alemayehu, K. E. Thomas, R. F. Einrem, A. Ghosh, *Acc. Chem. Res.*, 2021, **54**, 3095-3107.
- [8] A. Ghosh, J. Conradie, *J. Phys. Chem. A*, 2021, **125**, 9962-9968.

- [9] A. Ghosh, T. Wondimagegn, A. B. Parusel, *J. Am. Chem. Soc.*, 2000, **122**, 5100-5104.
- [10] A. Ghosh, *Chem. Rev.*, 2017, **117**, 3798-3881.
- [11] A. Alemayehu, J. Conradie, A. Ghosh, *Eur. J. Inorg. Chem.*, 2011, **12**, 1857-1864.
- [12] S. Ganguly, A. Ghosh, *Acc. Chem. Res.*, 2019, **52**, 2003-2014.
- [13] I. K. Thomassen, A. Ghosh, *ACS Omega*, 2020, **5**, 9023-9030.
- [14] A. J. McHugh, M. Gouterman, C. Weiss, *Theor. Chim. Acta*, 1972, **24**, 346-370.
- [15] A. Zhang, M. J. Stillman, *Phys. Chem. Chem. Phys.*, 2018, **20**, 12470-12482.
- [16] E. Fujita, C. K. Chang, J. Fajer, *J. Am. Chem. Soc.*, 1985, **107**, 7665-7669.
- [17] S. Licoccia, M. J. Chatfield, G. N. La Mar, K. M. Smith, K. E. Mansfield, R. R. Anderson, *J. Am. Chem. Soc.*, 1989, **111**, 6087-6093.
- [18] A. Ghosh, *J. Phys. Chem. B*, 1997, **101**, 3290-3297.
- [19] A. B. Parusel, A. Ghosh, *J. Phys. Chem. A*, 2000, **104**, 2504-2507.
- [20] N. C. Handy, A. J. Cohen, *Mol. Phys.*, 2001, **99**, 403-412.
- [21] C. Lee, W. Yang, R. G. Parr, *Phys. Rev. B*, 1988, **37**, 785-789.
- [22] S. Grimme, J. Antony, S. Ehrlich, H. Krieg, *J. Chem. Phys.*, 2010, **132**, article no. 154104.
- [23] H. Ryeng, E. Gonzalez, A. Ghosh, *J. Phys. Chem. B*, 2008, **112**, 15158-15173.
- [24] Y. Yakinaga, S. Ten-no, *Chem. Phys. Lett.*, 2008, **462**, 348-351.
- [25] G. te Velde, F. M. Bickelhaupt, S. J. A. van Gisbergen, C. F. Guerra, E. J. Baerends, J. G. Snijders, T. Ziegler, *J. Comp. Chem.*, 2001, **22**, 931-967.
- [26] A. Klamt, G. Schüürmann, *J. Chem. Soc., Perkin Trans.*, 1993, **2**, 799-805.
- [27] J. Conradie, C. C. Wamser, A. Ghosh, *J. Phys. Chem. A*, 2021, **125**, 9953-9961.